2021 NA62 Status Report to the CERN SPSC

Abstract

The status of the NA62 experiment is reported. The ongoing activities on detectors and hardware are summarised, together with our plans for the restart of data taking in July 2021. Results of the $K^+ \to \pi^+ \nu\bar{\nu}$ analysis based on the 2016-2018 Run1 data set are reported, and prospects for 2021-2024 Run2 are presented. Highlights of rare and forbidden decay analyses and exotic searches are also briefly discussed.

CERN-SPSC-2021-009 / SPSC-SR-286
30/03/2021

1 Introduction

Since the previous report in April 2020, the NA62 experiment analyzed the data collected in 2018. The NA62 Run1 (2016-2018) $K^+ \to \pi^+\nu\bar{\nu}$ result, combining the 2018 data with the previous data sets, was presented at the ICHEP2020 International Conference and at a CERN EP Seminar in Autumn 2020, is available on arXiv [1] and has been submitted to JHEP for publication. The result is the most precise determination of the $K^+ \to \pi^+\nu\bar{\nu}$ decay rate to date and provides the strongest evidence so far (3.4 σ) for the existence of this process. The Run1 data also allow NA62 to achieve the best sensitivity for the search of $K^+ \to \pi^+ X$ where X is a scalar or pseudo-scalar particle. Several other results on rare and exotic processes have been achieved, and published.

The NA62 Collaboration submitted an Addendum in 2019 [2], to continue the data taking of the experiment during the period after CERN Accelerators Long Shutdown 2 (LS2) and before Long Shutdown 3 (LS3). Our physics goals for the upcoming years are to perform a measurement of the branching ratio of the ultra-rare $K^+ \to \pi^+\nu\bar{\nu}$ decay with significantly improved accuracy, to substantially increase the sensitivity on several rare and forbidden kaon decays, and to reach unprecedented sensitivity in the investigation of several Standard Model (SM) extensions involving faintly interacting long-lived particles. To reach these goals, the NA62 experiment is fully committed to take data until LS3 (Run2). The NA62 experiment will restart data taking imminently, with a beam allocation of 168 days from July to November 2021. The FRC of November 2020 approved the budget for 2021, and the forecast for 2022.

During 2020, the $K^+ \to \pi^+\nu\bar{\nu}$ analysis strategy has been focused on further improving the signal sensitivity as well as fully exploiting the existing data sets. The experiment has invested significant resources to improve the Monte Carlo simulation, including the simulation of the pileup. The preparation for the restart of data taking has progressed, despite the global persistent pandemic. This report offers a summary of the $K^+ \to \pi^+\nu\bar{\nu}$ analysis based on Run1 data, and presents our plans and prospects for Run2. Thanks to a substantial analysis effort, several additional physics analyses are ongoing, spanning precision measurements and searches for exotic processes.

The document is structured as follows: Sections 2, 3 and 4 summarise the ongoing activities on the hardware, the data quality and simulation; the $K^+ \to \pi^+\nu\bar{\nu}$ analysis on the 2016-2018 data, and plans and prospects for Run2 are described in Section 5. Sections 6 and 7 report current highlights of rare/forbidden decays and exotic searches, respectively. Finally, the list of recent publications is presented in Section 8.

2 Status of the detector and on-going activities

A description of the detector can be found in [3] and a schematic is shown in Fig 1.

Despite the difficulties caused by the pandemic to the manufacture of new equipment and to the installation and testing of hardware and software at CERN, the collaboration will be ready to re-start the experiment when the SPS beam arrives in July 2021.

Several maintenance activities and interventions have been scheduled for Spring 2021. The major maintenance operation concerns the vacuum system. In particular, the cryo-pumps of the vacuum system will undergo a thorough check and replacement of key components by an outside company. This will allow efficient operation of the vacuum system until LS3. This intervention was originally foreseen in 2020, but it has been re-scheduled for April 2021 due to COVID-19.

In order to reduce the background contamination to the measurement of the $K^+ \to \pi^+\nu\bar{\nu}$ decay, it was decided to modify the beam layout upstream of the decay volume. The main changes are: an optimized achromat; a 4th GTK station (GTK0), placed next to GTK1; a new veto-counter (Veto) around the beam pipe before and after the collimator. The purpose of the Veto stations placed upstream of the final collimator is to detect charged pions and photons from upstream kaon decays. In addition, the new hodoscope (Anti0), mainly against the muon halo background present in dump mode searches, has been completed and will be installed for the next data taking, at the entrance of the fiducial volume (see Figure 2). The Anti0 may also help with the reduction of background trigger rates in the kaon mode.

The new layout (see Figure 2) has been designed after extensive simulation to quantify the expected background reduction (see Section 5). The position of the various beam components and vacuum sections in the modified beam line have been determined and the new vacuum sections have been produced. The new elements of the modified beam line will be installed in March and April 2021, including the installation of the Anti0. The fourth cooling line for GTK0 and the modifications to the cooling station have been completed. A pre-production of the scintillators for the Veto has been produced and validated. The production of the detector parts has started and is on track to have the Veto ready and installed before the start of data taking.

Over the last several years, small leaks were found and fixed on the LKr calorimeter requiring detector top-up with clean krypton. The level of the liquid Krypton in the LKr detector has been stable since the summer of 2017, with a minor leak appearing in 2020. The leak was found and repaired. Twenty-four bottles of krypton, or about 400 litres of liquid, were bought in 2017 to replenish the detector and partially refill the existing storage dewar (the overall LKr volume of the detector is 10000 litres). It was decided to make use of these 400 litres to top-up the calorimeter during LS2.

Since the supplied gas comes with ppm impurity level, it has to be purified to the ppb level by a series of gas-phase filters before being transferred to the detector. A small LKr time projection chamber was constructed to validate the purity of the krypton after the filters by measuring the lifetime of the drift electrons. The chamber was installed in a 2.5 litres cryogenic vessel placed next to the LKr in collaboration with the CERN cryogenics group. The device, which is triggered by scintillation light using SiPMs, measures the collected charge from a ^{22}Na positron annihilation gamma ray source as a function of the electron drift time, to obtain the ionization electron attenuation length and estimates of the purity. In Autumn 2020 the purity monitor itself and the purity of the Krypton was validated: all bottles were sampled, and the impurity level after the filters was found to be roughly one ppb, well within requirements for the NA62 LKr calorimeter. The remnant contents of the storage dewar were also sampled, bypassing the filters, and found to be heavily contaminated. Consequently, it was decided to refill the detector directly via the filters, avoiding the storage dewar. Approximately 180 litres were then transferred to the LKr calorimeter and the rest was transferred to the Krypton storage dewar. Subsequent measurements will determine the level of contamination in the Krypton from the dewar after first passing through the filters and the procedure to adopt for transfer to the LKr calorimeter. In addition, a pressure sensing device connected to the DCS has been installed in order to monitor the leak-tightness of the two leaking flanges of the LKr system.

2.1 Sub-Detectors

The regular maintenance and interventions on the detector included the replacement of ageing SiPM in CHANTI, and the replacement of the RICH HV mainframes (two out of four were replaced already in April 2019), given that maintenance of the old type is no longer guaranteed by the manufacturer. The RICH neon quality is routinely monitored; if needed in the future, one full neon fill is available. The recovery of the very few problematic channels in LAVs and in STRAW chambers is planned for Spring 2021.

As mentioned above, the GTK has been extended from three stations to four. Based on previous experience, 8 detector modules per year (4 in the beam + 4 spare) are needed. Considering

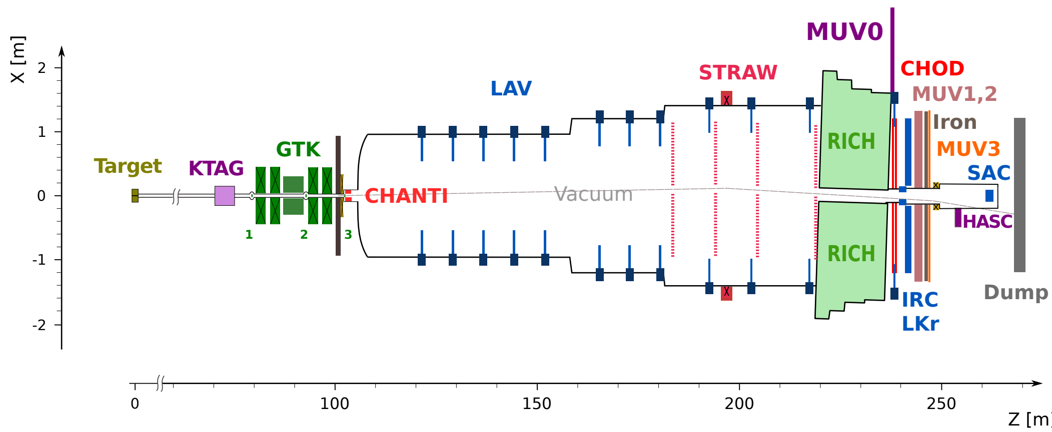

Figure 1: Layout of the NA62 experiment. KTAG: differential Cherenkov counter; GTK: Si pixel beam tracker; CHANTI: ring stations of scintillator bars; LAV: lead glass ring calorimeters; STRAW: straw magnetic spectrometer; RICH: ring imaging Cherenkov counter; MUV0: off-acceptance plane of scintillator pads; CHOD: planes of scintillator pads and slabs; IRC: inner ring shashlik calorimeter; LKr: electromagnetic calorimeter filled with liquid Krypton; MUV1,2: hadron calorimeter; MUV3: plane of scintillator pads for muon veto; HASC: near beam lead–scintillator calorimeter; SAC: small angle shashlik calorimeter. In the layout, the final fixed collimator installed in 2018 is visible, between GTK and CHANTI.

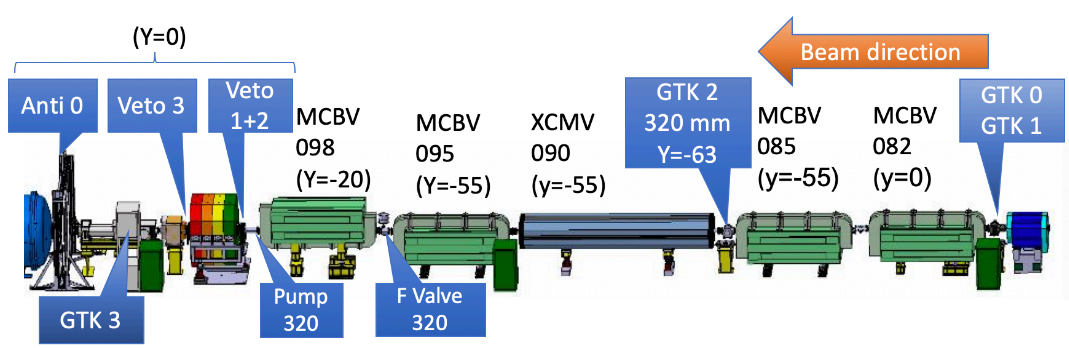

Figure 2: Schematic layout of the new achromat and beam line.

some contingency in fabrication and operation, the fabrication of 16 new modules is planned to cover data taking after LS2. Orders for all the required parts have been placed and the detectors required for the start-up in 2021 have been assembled. Our present fabrication rate is based on six detector modules per year, and the detector modules (including spares) should be completed in 2022.

A new high-voltage connector for the LKr detector has been developed in collaboration with LEMO after repeated vacuum leaks in the high-voltage feedthroughs. At present there are no apparent leaks and the replacement of connectors will only happen if there are new leaks. Spares are available for all parts of the calorimeter read out.

The HASC has been proven to be effective as a photon veto complementary to the LAV, LKr, IRC and SAC calorimeters (see Section 5). Given the success of the HASC as photon veto, a duplication of the detector is planned, in a symmetrical position with respect to the beam axis The nine modules for the second HASC station have been procured and the support structure is completed. The modules will be installed and integrated before the start of data taking.

The NA62 experiment was designed to tag beam kaons using a CEDAR Cherenkov detector filled with gaseous hydrogen as the radiator, and to this end CERN provided the necessary hydrogen infrastructure together with the extensive safety infrastructure required. Early simulation work showed that the CEDAR-W filled with nitrogen, for which the optics was designed to correct both spherical and chromatic aberrations, would meet the design specification in terms of efficiency and time resolution, and subsequent measurements with data have amply confirmed this. Because of the different chromatic dispersion of hydrogen, merely replacing nitrogen as the radiator in the CEDAR-W would result in a broadening of the Cherenkov cone and the overlapping of light from pions with that from kaons. To prevent this from happening, only a fraction of the kaon light could safely have been used and the reduction in the number of detected photo-electrons would have severely compromised the detection efficiency for kaons. As such, the NA62 KTAG has used the CEDAR-W filled with nitrogen for the whole of Run1.

Using hydrogen, rather than nitrogen, as the radiator would reduce the beam-gas scattering and as the sensitivity of the experiment continues to increase so do the physics concerns about the potentially harmful effects of this scattering. In April 2019, the BE-EA group identified a spare CEDAR and recovered the 40-year-old design drawings, the study of which has enabled the former mechanical and optical knowledge to be safeguarded by CERN. Physicists working with the BE-EA group have designed new lenses to reduce the aberrations for a hydrogen radiator and, with other small modifications, have produced an overall design, called CEDAR-H, that maintains the high performance of the nitrogen radiator.

With continued CERN support we are thus in a position to adapt CEDAR-H to the modern photo-detection system of KTAG and complete the installation for which the hydrogen infrastructure was implemented. Physicists will continue to work with the BE-EA group on the optical alignment of CEDAR-H, which requires very high precision, and once new lenses have been installed will take responsibility for testing CEDAR-H prior to commissioning it on the beamline. In light of the benefit to the experiment we will work with CERN towards installing CEDAR-H as soon as possible, and at the latest by 2023. Once this is done the existing CEDAR-W filled with nitrogen will be available as a fully operational spare to mitigate the risk of relying on such a unique instrument that is essential for the $K^+ \to \pi^+ \nu \bar{\nu}$ analysis.

2.2 TDAQ

The preparation for the coming data taking has continued. Dry runs with experts largely working remotely have been organised, to investigate and address improvements to the TDAQ system.

An addition to the L0 calorimeter trigger in terms of a condition based on total calorimetric energy, using information from MUV1/2, and of a di-electron trigger, based on topological information from the electromagnetic clusters, is planned for late Spring 2021. The readout of the energy and position of the clusters, to be used by the L1 trigger, will also be commissioned in Spring. A GPU-based L0 trigger using RICH information is under development, to improve the selectivity of the trigger for rare kaon decays with an electron in the final state, and has been tested with simulated data. Its implementation will be first tested, in parallel to the current triggers, at the beginning of the data taking and then deployed once validated.

A Trigger Burst Emulator (TRIBE) has been prepared to study the behaviour of the L0TP, including the emulation in high intensity conditions. The replacement of the L0TP processor (L0TP+) based on a more modern FPGA will be installed in parallel to the L0TP and validated with beam, for a possible substitution once validated.

There have been several studies in the laboratory, using the data collected in 2018 and emulators, to study the rate limitations exhibited during nominal-intensity tests and improve the efficiency of the GTK readout, including the resilience of the firmware to intensity peaks. Further tests are foreseen for Spring 2021, and a version of the firmware that improves on the limitations will be installed before data taking. The new prototype FPGA-based TDC system (higher rate, no dead time) readout by the ATLAS Felix board into a computer will be installed for the Veto counter.

The Run Control of the experiment has been upgraded with the addition of the new detectors. A detailed offline analysis of the available monitor data for the 2018 run was performed, with the purpose of defining useful quantities and the best procedure for an online monitor for the overall TDAQ efficiency. Based on this investigation, a new subsystem has been prepared in the Run Control, based on data collected by various subsystems and presented as a series of plots. This new feature has been tested in a recent dry run. The information will be available to the shift crew in real time and also accessible from remote.

The Online monitor program has been rewritten to improve the speed of processing for a fast response and to improve the interaction of the operator with the graphics presentation, optimizing the quantity and the size of the histograms for a faster access.

Several upgrades has been made to the readout infrastructure: renewing of old service computers; new network switches for a better and more reliable connection; cleanup of network cabling; complete cabling of CHOKE connections from the various readout units and their check, including a complete check-up of the CHOKE signals from the calorimeter readout; availability of a good number of spares for TEL62 and TDCBs. The CHOKE is a warning signal sent by detectors when their buffers are almost full; it is detected by the L0TP, that then stops dispatching triggers until the critical period has ended. The importance of using the CHOKE lines was demonstrated in 2018, albeit with only few detectors connected, and the CHOKE system is now fully deployed.

Given the fast-changing and unsettled international travel situation we have devised a scheme to control the experiment and take data with an optimized schedule for in-person shifts, run coordinators and experts. In particular, to facilitate the interaction with experts who could be forced to work only remotely, we are setting up a series of tools: a high quality camera installed in the control room, able to zoom on the various screens, to allow the remote expert to follow the activity of the run; an audio station connected to a computer for a reliable Zoom interaction; a portable camera, likely a smartphone on an helmet, wearable by the general experts in case of intervention in the experimental area, to allow the remote experts to follow the operation. Vital online data quality checking has been redesigned so that it can be also accomplished remotely.

3 Data Quality and Data Processing

The full 2016-2018 NA62 data set has been successfully processed in the foreseen timescale, using new calibration procedures and substantially improved reconstruction software.

The individual time resolution of KTAG and RICH is ~ 70 ps, while for a long time the resulting resolution of the KTAG-RICH time difference was about 130 ps instead of the expected 100 ps. The reason for this degradation in time resolution was finally understood and traced back to the non-linearity of the HPTDC chip when used in the "high-performance" mode, which effectively introduced a jitter with a dependence on the measured fine time. After understanding the root cause of the issue, a new set of corrections was introduced, which realign the event-by-event times depending on the event fine time. With these new corrections, the time resolution of the KTAG-RICH system finally reached the expected 100 ps.

The LKr reconstruction software, a left-over from NA48 and still written in FORTRAN, has been fully imported to C++, substantially improving the structure and the readability. This work allowed us to review in detail the most hidden aspects of the code and several important issues which were preventing optimal performance at high beam intensity were corrected. Furthermore, the present reconstruction does not resolve well clusters occurring in the same spatial region but at several tens of ns away, because the fast ADC sampling time (25 ns) is comparable with the cluster separation. A major revision of the LKr reconstruction is in progress, aiming at reducing substantially the mis-reconstruction of this event topology.

The above-mentioned improvements are essential to enable the experiment to handle the higher beam intensity proposed for 2021. The estimate of the expected data rates and resources needed for the 2021-25 data taking is based on 2018 data. In 2021-25 we expect similar rates of raw data despite the higher intensity, as the L0 bandwidth was saturated in 2018. This means that the total data size should scale with the number of days NA62 will be receiving beam. For 2021, 168 days of data taking have been assigned to NA62 (compared to 218 days in 2018). For the following years we assume an assignment similar to 2018. From the latest processing of 2018 data, in which the so-called "Slim Persistency" (a reduced output format introduced in 2019) was fully employed, we find that the output which goes to EOS is about 61% of the raw data size; during the processing itself some intermediate files of larger size are kept, but these are removed at the end. With these assumptions, a total raw data size to CTA of 1660 TB is expected for 2021, and 2150 TB for each of the years 2022-2025, with a total size of about 15 PB at the end of 2025 for all the data taken in 2014-2025. For EOS we project that about 1 PB will be needed for the 2021 data, and additional 1.3 PB for each of the following years. Additionally, some dedicated EOS space will be needed to accommodate the change in the tape writing scheme, due to the transition from CASTOR to CTA, as we have fully migrated from CASTOR to CTA in March 2021. Taking all of the above into account, at the end of 2025 NA62 data is expected to occupy about 10 PB of EOS space. NA62 total allocation at the beginning of March 2021 was 4 PB, which was almost fully occupied by the processing outputs. In the short term, and for the preparation of the 2021 data taking, an increase of 1 PB was requested to CERN IT, which was granted shortly after and fully applied on the 11^{th} of March 2021. On that occasion, we also asked for an additional 1 PB to be applied later in the year, and such request was also approved. As for processing power (HTCondor) we expect that no additional resources are needed, i.e. our current quota assignments will be sufficient.

All these future projections will be refined, in particular after the number of allocated beam days in every single year will be known. We would like to express our gratitude to the IT Department for their support and expertise in assisting the needs of the experiment, and in particular to Xavier Espinal and Bernd Panzer-Steindel, for the excellent support and services provided to NA62.

4 Monte Carlo simulation

The Monte Carlo (MC) software was significantly improved and extended in functionality during last year. In order to obtain a much higher statistics in MC productions for specific needs, several new biasing methods were introduced. Some of them exploit Geant4-based techniques to enhance the cross-section of certain rare processes: the simulation of rare inelastic interactions in the GTK, requested for a more effective background reduction and estimation in the $K^+ \to \pi^+\nu\bar{\nu}$ analysis, or the $K^+ \to \pi^+\pi^0$ sample with enhanced photon conversion in the STRAWS for the ongoing $\pi^0 \to e^+e^-$ analysis are examples of this category. Others, instead, act directly at the decay generator level (phase space, capped lifetimes) to generate only the interesting events, as in the case of the simulation of biased $K^+ \to \pi^+\pi^0$ decays with at least a photon emitted in the small-angle veto region, or in the case of $K^+ \to \mu^+\nu$ decays with capped muon lifetime and subsequent $\mu^+ \to e^+\nu\bar{\nu}$ decay.

Another improvement, though the validation is ongoing, is the replacement of the K12 beamline simulation with G4beamline by a recent detailed model employing the BDSIM software [4]. The BDSIM software is based on Geant4, incorporating most of its flexibility but being optimized for the specific use case of accelerators. It thus provides accelerator-relevant analysis output and settings, as well as a proper treatment of magnetic field maps. The BDSIM model of the K12 beamline has been created and is maintained by the BE-EA group. The K12 simulation will provide the necessary beam background input to NA62MC via the proton-on-target/-on-TAX collision simulation and propagation of all particles to the NA62 experiment entry. In addition, it allows for studies to reduce the muon flux in the detector, for kaon beam and beam dump modes; such studies are currently being performed in collaboration with the BE-EA group.

The NA62 MC production is performed in two steps: firstly, the generation of the physics and the subsequent propagation of particles through the detectors; secondly, the digitization with the following reconstruction. Since the digitization and reconstruction software version changes more often than the geometry or the generators, due to the iterative validation process with data, an automatic re-processing framework was set up, based on the existing re-processing framework for data. This allows for re-reconstructing the existing MC samples on short time scales without needing to regenerate new productions, and for executing automatic calibration steps, similar to those performed for data. In order to reduce the output file size, a so-called "slim" format was introduced for MC, in a similar way as it was done already for data. To monitor the quality of MC productions, a web-based comparison tool has been created, that publishes the relevant distributions for each detector and common decay selections. In addition a regular monitoring of the acceptances of particular decay channels is performed as soon as a new revision is released.

In preparations for Run 2, the simulation is being finalized, incorporating the new detectors (Veto counter, Anti0, HASC2) and the modified beam line configuration.

5 Status of the $K^+ \to \pi^+\nu\bar{\nu}$ analysis

The theoretical prediction of the $K^+ \to \pi^+\nu\bar{\nu}$ decay branching ratio is subject only to a small uncertainty [5, 6, 7, 8, 9, 10]. This decay is among the most promising modes to search for non-Standard-Model signals in flavour physics, as it probes higher mass scales than other rare meson decays, and several models foresee deviations from Standard Model predictions [11, 12, 13, 14, 15, 16, 17, 18, 19, 20].

Data taken in 2018 have been fully analysed, and the preliminary result was reported at the ICHEP2020 conference [21] together with the combination of the results from the 2016 and 2017 analyses. The final result has been released recently [1] and submitted to JHEP. The branching ratio, measured on the 2016-2018 (Run1) data sets, is:

$$\mathcal{B}(K^+ \to \pi^+\nu\bar{\nu}) = \left(10.6^{+4.0}_{-3.4}\big|_{\mathrm{stat}} \pm 0.09_{\mathrm{syst}}\right) \times 10^{-11} \quad \text{at} \quad 68\%\text{CL}. \tag{1}$$

The result is the most precise determination of the $K^+ \to \pi^+\nu\bar{\nu}$ decay rate to date and provides the strongest evidence so far for the existence of this process.

The $K^+ \to \pi^+\nu\bar{\nu}$ analysis ("PNN analysis") was carried out on a $K^+ \to \pi^+\nu\bar{\nu}$ triggered data stream ("PNN data"), as in the 2016-2017 analyses. Minimum-bias data were also used for normalization and background studies.

The 2018 analysis took advantage of an overall optimization of the analysis with respect to that of the 2016-2017 data. The improvements led to a sizable increase in the signal acceptance, while keeping the same level of signal-over-background ratio. The best analysis performance was obtained for data collected after June 2018, which profited from the newly installed final collimator. This sample corresponds to about 80% of the 2018 data and is referred to as S2 below; the sample of data collected before June 2018 is referred as S1.

Table 1 shows a comparison of the 2016, 2017 and 2018 analysis performances. The invariant mass squared of the $\nu\bar{\nu}$ pair, also termed m^2_{miss}, characterizes the kinematics of signal and background events. Denoting p_π the π^+ momentum, the plane (p_π, m^2_{miss}) was divided in regions. The signal was looked for into two regions, called Region 1 ($0 < m^2_{miss} < 0.01\,\mathrm{GeV}^2/c^4$) and Region 2 (above $0.026 < m^2_{miss} < 0.068\,\mathrm{GeV}^2/c^4$). Depending on the type of events, the other regions were used for background normalization ("background region") or to test the background prediction ("control regions").

5.1 Optimization of the $K^+ \to \pi^+\nu\bar{\nu}$ selection

Several improvements in the 2018 selection criteria led to the increase of signal acceptance with respect to the 2017 analysis.

The p_π range of the accepted events in Region 2 was extended from 35 to 45 GeV/c. The power-like increase of the $K^+ \to \mu^+\nu$ background with p_π prevented a similar extension for Region 1. The 15–45 GeV/c p_π range was divided in 6 momentum bins, 5 GeV/c wide, and the selection criteria optimized in each bin separately.

The cuts on the longitudinal position of the reconstructed K^+ decay vertex (Z_{vtx}) defining the fiducial volume (FV) depended on the π^+ momentum bin. The FV of events with $p_\pi <$ 20 GeV/c was decreased to reduce the $K^+ \to \pi^+\pi^0$ background. The FV of S2 events with p_π from 20 to 35 GeV/c was extended by 5 m downstream towards the first STRAW chamber. A condition on the maximum Z_{vtx} versus π^+ momentum applied in previous analyses against the $K^+ \to \pi^+\pi^+\pi^-$ events was released. All these modifications led to an overall increase of the FV in 2018.

The analysis of the 2016–2017–2018(S1) relied on the π^+ position at the transverse plane of the final collimator (x_{col}, y_{col}) to suppress upstream events. This required the rejection of events falling outside a rectangular (x_{col}, y_{col}) region centred on the beam axis and $100 \times 400\,\mathrm{mm}^2$ wide. The y cut was driven by the geometry of the old adjustable collimator, that in data prior to S2 left central corridors along y through which π^+ mesons produced upstream could enter the FV. This rectangular cut, also called "box cut", contributed to about 40% of signal loss and did not leave any room for optimization of the upstream events rejection. The final collimator installed in June 2018 prevented π^+ mesons produced upstream from entering the FV from above or below the collimator beam hole, giving room to reduce the box cut. This allowed the use of additional variables against upstream events, namely the x, y, z coordinates of the decay vertex, the π^+ track slopes and positions at the first STRAW chamber. Therefore, the selection of S2 events exploited a newly developed Boosted Decision Tree (BDT) algorithm that took over the role of the box cut.

The negligible background from kaon decays with μ^+ or e^+ in Region 2 achieved in the 2016–2017 analyses allowed for an educated softening of the conditions of π^+ identification in the 2018 data analysis. The π^+ identification criteria with calorimeters and RICH were optimized separately for each bins of π^+ momentum and for S1 and S2. In addition, the 2018 analysis profited from an improved training of the BDT classifier that exploited calorimetric

Table 1: Summary of the analyses of the 2016, 2017 and 2018 data. SES indicates the single event sensitivity. The numbers of expected signal events assume a SM signal branching ratio equal to $(8.4 \pm 1.0) \times 10^{-11}$; the uncertainties on the expected signals do not include the error on the SM branching ratio. Observed candidates are the number of events in signal regions R1+R2 after the PNN selection. Signal acceptance does not include the contributions that cancel in the ratio to the normalization acceptance when computing the SES, like detector efficiencies; the uncertainty on the signal acceptance is dominated by the efficiency for particle identification and K/π association that largely cancel after normalization. RV (Random Veto) efficiency is the efficiency to select signal events after applying photon and multiplicity rejection criteria. The effective number of K^+ decays is inferred from the number of normalization events, without considering acceptance effects that cancel between signal and normalization. The third group of rows lists the different contributions to the total estimated background.

	S2 2018	S1 2018	2017	2016
SES$\times 10^{10}$	0.14 ± 0.01	0.54 ± 0.04	0.389 ± 0.024	3.15 ± 0.24
Signal expected (SM)	6.02 ± 0.39	1.56 ± 0.10	2.16 ± 0.13	0.27 ± 0.20
Background expected	$4.31^{+0.91}_{-0.72}$	$1.11^{+0.40}_{-0.22}$	1.46 ± 0.33	$0.152^{+0.093}_{-0.035}$
Candidates observed (R1+R2)	15	2	2	1
Signal acceptance $\times 10^2$	6.4 ± 0.6	4.0 ± 0.4	3.0 ± 0.3	4.0 ± 0.4
Trigger efficiency	0.89 ± 0.05	0.89 ± 0.05	0.87 ± 0.03	0.90 ± 0.03
RV efficiency	0.66 ± 0.01	0.66 ± 0.01	0.64 ± 0.01	0.76 ± 0.04
Effective K^+ decays $\times 10^{-12}$	~ 1.9	~ 0.8	~ 1.5	~ 0.12
$K^+ \to \pi^+\pi^0(\gamma)$	0.52 ± 0.05	0.23 ± 0.02	0.29 ± 0.04	0.064 ± 0.009
$K^+ \to \mu^+\nu(\gamma)$	0.45 ± 0.06	0.19 ± 0.06	0.15 ± 0.04	0.020 ± 0.007
$K^+ \to \pi^+\pi^-e^+\nu$	0.41 ± 0.10	0.10 ± 0.03	0.12 ± 0.08	$0.013^{+0.019}_{-0.013}$
$K^+ \to \pi^+\pi^+\pi^-$	0.17 ± 0.08	0.05 ± 0.02	0.008 ± 0.008	0.002 ± 0.002
$K^+ \to \pi^+\gamma\gamma$	< 0.01	< 0.01	0.005 ± 0.005	< 0.002
$K^+ \to \pi^0\ell^+\nu$ ($\ell = \mu, e$)	< 0.001	< 0.001	< 0.001	< 0.001
Upstream background	$2.76^{+0.90}_{-0.70}$	$0.54^{+0.39}_{-0.21}$	0.89 ± 0.31	$0.050^{+0.090}_{-0.030}$

variables to distinguish π^+ from μ^+ and e^+.

Photon rejection in LAV exploited in-time activity only in stations downstream of the K^+ decay vertex, contrary to the 2016-2017 analyses where all stations were considered. Studies on 2017 data showed that this new condition did not affect the upstream background. The new LAV veto criteria led to $\sim$5% absolute reduction of random signal losses ("random veto"). Besides, a new BDT classifier exploiting the nature of the energy release in LAV was studied to further optimize photon rejection. However, LAVs are relevant also to suppress events with multi-charged particles in final state, against which the BDT required a specific training that is currently under study.

The multi-charged particle rejection profited from a new algorithm to reconstruct track segments in the STRAW chambers. Track segments are efficient to veto events with additional charged particles missing two chambers for acceptance reasons. Compared to the previous algorithm developed in 2015, the new algorithm, optimized on 2017 data, allowed for a 3% absolute reduction of the random veto in 2018.

5.2 Signal and background measurements

The strategies to measure the single event sensitivity and to estimate the background were similar to those adopted in the 2017 analysis.

$K^+ \to \pi^+\pi^0$ decays selected kinematically served for signal normalization. The measurement of the trigger efficiency exploited samples of K^+ decays selected on minimum bias data. Normalization and signal acceptances resulted from MC simulations that included pileup activity in the detectors upstream of the fiducial volume. A sample of $K^+ \to \mu^+\nu$ decays allowed for the measurement of the signal losses due to random veto on data. As a consequence of the improvements on photon rejection described in Section 5.1, the fraction of signal lost because of random veto compared favourably with that of 2017 despite the higher beam intensity of the 2018 data.

The $K^+ \to \pi^+\pi^0$ and $K^+ \to \mu^+\nu$ background evaluation relied on data. The method exploited the independence between photon rejection and particle identification on one side and the kinematical definition of signal regions on the other side. Events of PNN data remaining in the $K^+ \to \pi^+\pi^0$ and $K^+ \to \mu^+\nu$ background regions after PNN selection were used for normalization. Minimum-bias data provided the measurement of the extrapolation factors (m^2_{miss} kinematic tails) from background to signal regions. A new procedure was developed to measure the kinematics tails of $K^+ \to \mu^+\nu$ events. This procedure increased the statistical uncertainty of the estimated $K^+ \to \mu^+\nu$ background, but avoided systematic effects due to the correlation between kinematics and particle identification.

Evaluation of the $K^+ \to \pi^+\pi^+\pi^-$ background relied on MC to measure the extrapolation factor from background to signal region, and on PNN data in the corresponding background region for background normalization. The larger $K^+ \to \pi^+\pi^+\pi^-$ background in 2018 required the development of a more accurate procedure for evaluation, compared to that of the previous analyses. Background from the $K^+ \to \pi^+\pi^-e^+\nu$ decay was estimated from MC normalized to $K^+ \to \pi^+\pi^0$ events. The larger background in 2018 than in 2016-2017 was a side effect of the modified selection criteria.

The evaluation of the upstream background followed the data-driven method developed for the 2017 analysis. The probability of K/π association in upstream events was measured using an upstream-enriched data sample selected by removing the CHANTI veto criteria. The background was normalized to a sample of upstream events selected on PNN data without requiring K/π association, separately for each bin of the difference of the K^+ time measured in KTAG and GTK. Accurate studies of the systematic effects due to the modelling of the K/π mis-matching probability were possible in 2018, thanks to the higher statistics available.

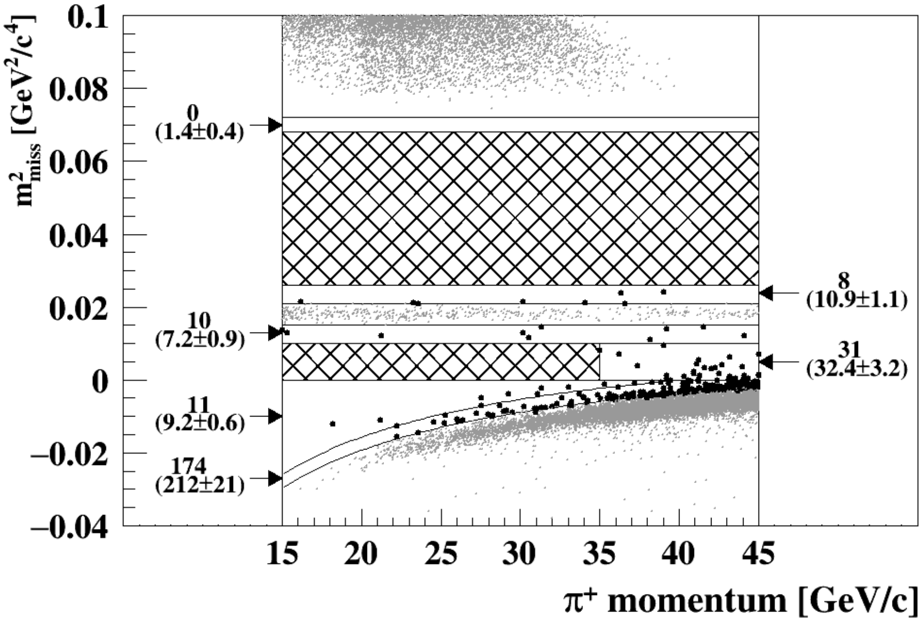

Figure 3: Reconstructed m^2_{miss} as a function of π^+ momentum after applying the signal selection to the S1 and S2 subsets. The background regions are displayed using light grey dots. The regions with the solid black markers adjacent to the background regions are the control regions. The numbers next to these regions are the expected number of background events (in brackets) and the observed number (without brackets).

The larger 2018 data-sets allowed statistically meaningful tests of the background predictions as a function of p_π in control samples and control regions. Control samples were used to test the predictions for $K^+ \to \pi^+\pi^-e^+\nu$ and the upstream backgrounds, and were selected by inverting cuts relevant for the suppression of the corresponding background. The tests were performed after the completion of the background evaluation, following the rules of a blind analysis. The numbers of events observed in all control regions (see Figure 3) and control samples [1] were statistically compatible with expectations.

5.3 Statistical treatment

Figure 4 (left) shows the observed events in the signal regions. The statistical analysis of the result followed the approach of a counting experiment. The shape of the m^2_{miss} was not used because of the uncertainty in the modelling of m^2_{miss} of the upstream background. The $p-$value of the observed events in the signal regions under the background-only hypothesis provided an evidence at 3.4σ significance for the $K^+ \to \pi^+\nu\bar{\nu}$ decay.

The 2018 data were divided in 7 categories: 1 category for S1 and 6 categories corresponding to the 6 p_π bins for S2. The 2016-2017 results were then added as two separate categories. The measurement of the branching ratio was extracted using a maximum likelihood fit to the 9 categories. Expected backgrounds and the single event sensitivity were included in the fit as nuisance parameters.

5.3.1 Limits on $K^+ \to \pi^+X$ decay rate

The result was also interpreted in terms of $K^+ \to \pi^+X$ decay, where X can be an invisible scalar or pseudo-scalar particle predicted in BSM models at low energies. The analysis in this case

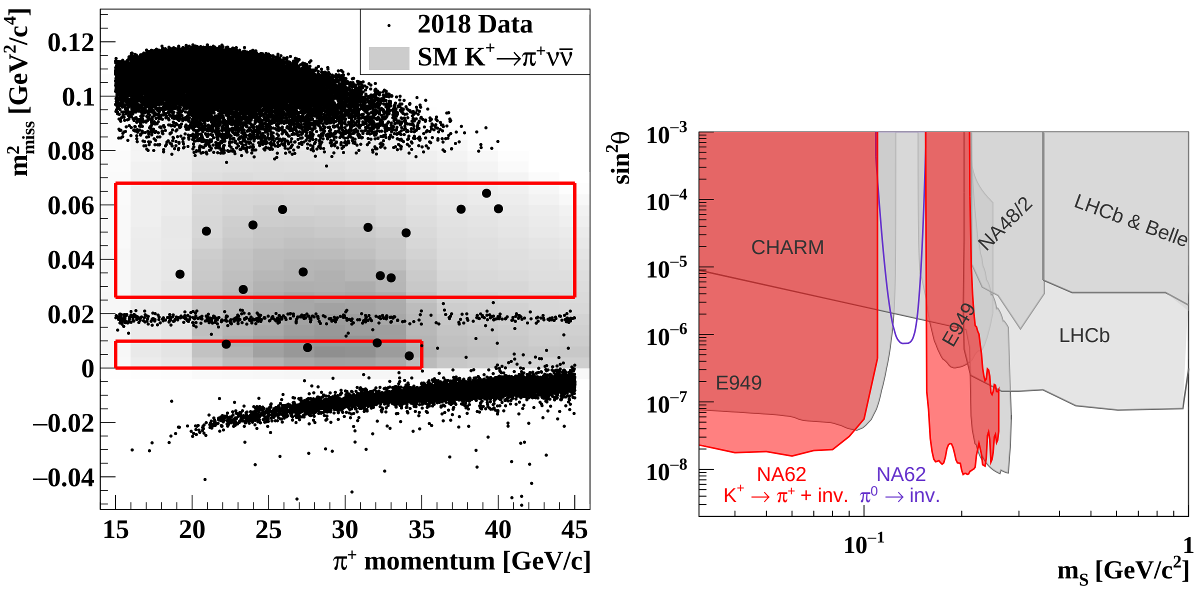

Figure 4: Left: Observed events in the signal regions in 2018 data set. Right: Exclusion plot for models in which X is a dark sector scalar mixing with the SM Higgs field according to the mixing parameter $\sin^2\theta$.

followed the strategy of a mass peak search, developed for the analysis of the 2017 data [22]. The dominant background to the $K^+ \to \pi^+ X$ decay is the $K^+ \to \pi^+\nu\bar{\nu}$ decay itself. The search is performed with a fully frequentist hypothesis test using a shape analysis with m^2_{miss} observable and an un-binned profile likelihood ratio test statistics. Upper limits on $K^+ \to \pi^+ X$ branching ratio excluding X at 90% CL for each X mass hypothesis are derived according to the CLs method. This result can be interpreted in several models predicting X particles. Figure 4 (right) shows the exclusion plot for models in which X is a dark sector scalar mixing with the SM Higgs field according to the mixing parameter $\sin^2\theta$. The region excluded from the recently published search for invisible π^0 decays is also shown.

5.4 Plans and prospects for Run2

The PNN analysis strategy is currently under revision in view of the upcoming data taking. The goal is to increase the signal acceptance while decreasing the background. Current studies focus on: the tuning of the analysis at full intensity; the development of more performant algorithms to improve specific areas of the analysis; background reduction using the new detectors, to be installed before July 2021.

The tuning of the analysis for the full intensity follows two paths. The first one is the reduction of the random veto losses that depend linearly on the beam intensity; the second one is the identification and modification of those parts of the analysis that show a dependence on the intensity, beside the random veto.

5.4.1 Random veto studies

The fraction of events lost because of random veto is measured on data using samples of $K^+ \to \mu^+\nu$ decays. The most relevant random veto effect as a function of the beam intensity is due to the photon rejection in the LKr. The main losses come from the width of the time windows (depending on the cluster energy), as large as ± 40 ns, to veto events with LKr clusters with energies above 10 GeV. Despite the sub-nanosecond LKr time resolution, such width is necessary because random clusters spatially overlapping with in-time clusters can result in time mis-reconstructions. Areas of possible improvements have been identified, and a major revision of the LKr reconstruction is ongoing, as mentioned in Section 3. First tests of the new reconstruction show a significantly improved capability to resolve spatially overlapping clusters separated in time, that can result in a reduction in the size of the veto timing windows. Independently from the revision of the reconstruction, algorithms based on Neural Network applied to computer vision are under study to identify and veto in-time clusters super-imposed on random activity in the LKr. Computer vision models based on SSD object detection algorithms [26], that make use of machine learning architectures like ResNet [24] or MobileNet [25], have been tested on 2017-18 data events with overlapping in-time and out-of-time activity. Preliminary results suggest the possibility to reduce the veto timing windows by at least a factor 4 for high energetic clusters, while keeping the same level of photon rejection efficiency. This alone would result in about 15-20% relative reduction of the LKr random veto losses. The combined use of the new LKr reconstruction and of the NN algorithm is envisaged to reduce the random veto losses in LKr up to a factor 2.

Studies, started last year, on the BDT to reject photons in the LAV are progressing. The main focus is to find an appropriate training sample that includes features to also reject events with multi-charged particles in the final state. The possibility to use overlay Monte Carlo [23] for this purpose is under study.

5.4.2 Signal acceptance increase

Intensity effects on signal acceptance beside random veto are investigated with the overlay MC [23]. Several studies are on-going to validate the overlay MC with data. The measurement of the fraction of events lost because of random veto is a powerful tool for this purpose. Preliminary results show that the overlay MC reproduces within 15% relative precision the drop of signal efficiency observed in data due to random losses as a function of the intensity. A detailed investigation of the spatial distribution of the random particles is on-going.

A first attempt to run the PNN analysis on overlay $K^+ \to \pi^+\nu\bar{\nu}$ MC did not reveal selection criteria particularly vulnerable to beam intensity. In addition, the overlay MC study has indicated the following areas where improvements in the $K^+ \to \pi^+\nu\bar{\nu}$ acceptance are possible: timing conditions, K/π association, fiducial volume definition, particle identification.

The timing conditions between Gigatracker, KTAG and CHOD detectors will be reviewed and consequently the impact of the CHOD detectors to the PNN analysis reduced.

A revision of the K/π association criteria is on-going in view of the expected reduction of the upstream background. The presence of an accidental beam track taking the role of the missing parent K^+ track is a feature of the upstream background, which motivates the tight association criteria. After the reduction of the upstream background by the new Veto, the K/π association is expected to have an impact mainly on the $K^+ \to \pi^+\pi^0$ and $K^+ \to \mu^+\nu$ backgrounds. Here, the backgrounds arise because the m^2_{miss} can be mis-reconstructed if an accidental beam particle has by chance a better matching quality than the parent K^+. However, the use of both the best and second-best association quality for GTK tracks is a powerful tool to allow a softening of the conditions while keeping the same level of background rejection. Preliminary studies show that it is possible to recover some % of relative signal acceptance from K/π association, independently of beam intensity.

The reduction of the upstream background could also lead to an increase of the fiducial volume. This possibility is studied with a softening of the upstream reduction criteria based on the BDT algorithm developed for the 2018 data analysis. The fiducial volume will increase towards the last GTK station. However this requires an accurate investigation of the background from particle interactions in the last GTK station, which is currently on-going.

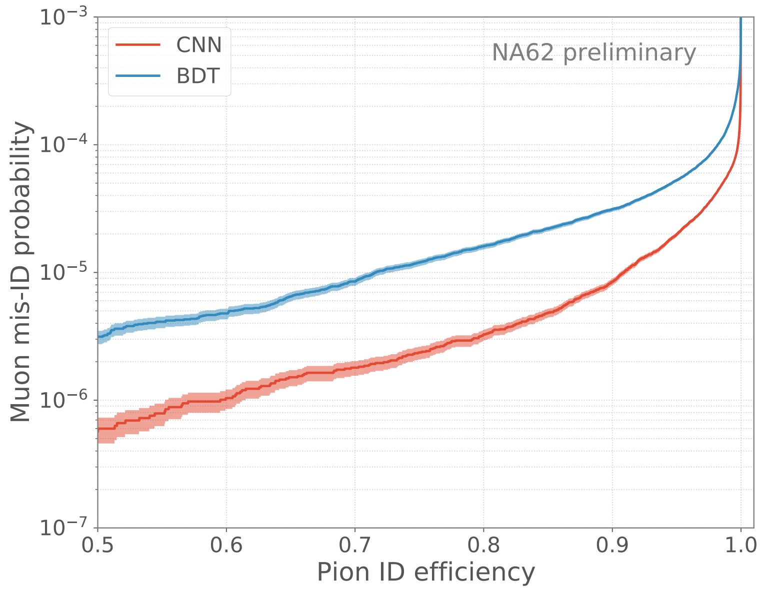

Figure 5: Calorimeter muon mis-ID probability as a function of the pion ID efficiency for events with momentum in the 15 to 50 GeV/c range. The newly developed CNN method is shown in red and the existing BDT based approach is indicated in blue. Those curves were obtained with the 2018 data set.

A new algorithm for particle identification with the calorimeter based on NN has been developed. Particle identification, particularly μ^+/π^+ separation, is crucial to NA62 measurements of $K^+ \to \pi^+\nu\overline{\nu}$ and is based primarily on RICH and calorimetry information. A new machine learning (ML) algorithm has been developed to extract particle identification (PID) information directly from the raw calorimeter hits. Previously, a boosted decision tree (BDT) approach based on reconstructed quantities was used.

High purity samples of events with a single muon, pion or electron track in the detector acceptance were extracted from the 2016, 2017 and 2018 NA62 data for the training and validation of the ML methods. An independent test sample was set aside and used for the final evaluation of the models. Easily identified muon events are filtered out at the beginning of the processing pipeline in order for the ML algorithm to focus on the most difficult cases to classify. A convolutional neural network (CNN) architecture based on the ResNet-18 network [24] was found to achieve the best μ^+/π^+ separation.

As shown in Figure 5, the evaluation of the method on an independent test data set indicates that the overall pion ID efficiency can be increased from 72% to 92% in the 15 to 50 GeV/c track momentum range while keeping the muon mis-ID probability at 1×10^{-5}. The positron mis-ID probability (not shown) is slightly improved. The new method will be applied to future analyses.

5.4.3 Background reduction

As anticipated in the previous Sections, improvements to the NA62 experimental setup are foreseen from 2021 aiming to further suppress the upstream background and the background from $K^+ \to \pi^+\pi^0$ decays.

The upstream background will be addressed by modifying the beam line region upstream of the third station of the GTK. Simulation studies validated on data indicate that the major source of the upstream background originates from $K^+ \to \pi^+\pi^0$ and $K^+ \to \pi^+\pi^+\pi^-$ decays inside the two magnets, B5 and B6, of the achromat used to measure the K^+ momentum. The charged π^+ is then transported inside the fiducial region and the rest of the decay products are absorbed by the material upstream of the last GTK station. An accidental track is selected in the GTK and matched to the π^+ creating a background source. The new Veto counter, designed to detect these decays, comprises three layers of scintillating tiles read out by SiPMs, alternated with absorber layers, to provide optimal sensitivity for photon and pion detection. The first two scintillating layers will be placed upstream of the final collimator. The third layer will be placed downstream of the final collimator to reduce random veto coming from the beam μ halo. In addition, the B5 and B6 magnets will be moved upstream to allow sufficient space for the decay products to exit the beam pipe before the position of the first two Veto planes, so they can be efficiently detected. A new GTK station will be added in front of the present GTK1 which will improve the treatment of accidental activity in the GTK and help further reduce the upstream background by improving the GTK time resolution and efficiency. The suppression factor of these modifications to the NA62 experimental setup will reduce the amount of upstream background by three to ten times, making the upstream background contribution subdominant with respect to the kaon decays component. A particular benefit of the upstream background reduction is that this leads to an overall more precisely known background. Because the kaon decays background is estimated with better accuracy than the upstream, the reduction of the upstream background gives the possibility to optimize the selection, allowing more background in the signal region, while simultaneously increasing the signal acceptance. To this end, the precise reconstruction of the distribution of the m^2_{miss} of the background from kaon decays opens the possibility to extract the branching ratio from a fit to m^2_{miss} for each momentum category, therefore boosting further the sensitivity to the signal.

Another detector will be added downstream of the muon veto (MUV3) and upstream of the beam dump. This detector has the same structure as the existing HASC and will be placed on the other side of the beam pipe at the same z location. The detector will provide suppression of electrons produced by interactions of high energy photons with the RICH beam pipe. The resulting electrons propagate inside the beam pipe and exit after they are deflected by the last dipole that transports the positively charged beam to the beam dump. The detection of the electrons will provide up to two-fold suppression of high energy photons and improve the π^0 rejection at low π^+ momentum. This will reduce the $K^+ \to \pi^+\pi^0$ background, which is the dominant source of K^+ decays background for the $K^+ \to \pi^+\nu\bar{\nu}$ measurement.

6 Rare and forbidden decays

A number of pre-scaled auxiliary trigger chains operating along with the main $K^+ \to \pi^+\nu\bar{\nu}$ trigger allowed for a broad rare decay physics programme. Multi-track L0 triggers for collection of K^+ decays to lepton pairs (i.e. di-muon, di-electron and muon-electron pairs) are based on RICH and CHOD multiplicity requirements, as well as the total LKr energy deposit and MUV3 signal multiplicity conditions. The corresponding L1 trigger performs beam kaon identification by the KTAG and online reconstruction of a negatively charged track in the spectrometer. The data set collected in 2016–18 with the di-muon trigger is equivalent to 3×10^{12} kaon decays in the vacuum tank upstream of STRAW1, while the data sets collected with the di-electron and electron-muon triggers are each equivalent to 10^{12} kaon decays. Additional data sets collected with minimum bias trigger conditions are equivalent to over 10^{10} kaon decays.

The record size of the dataset is complemented by the excellent kinematic resolution, particle identification and photon veto capabilities of the NA62 detector, leading to favourable background conditions. This allows for measurements of a broad range of K^+ and π^0 decays,

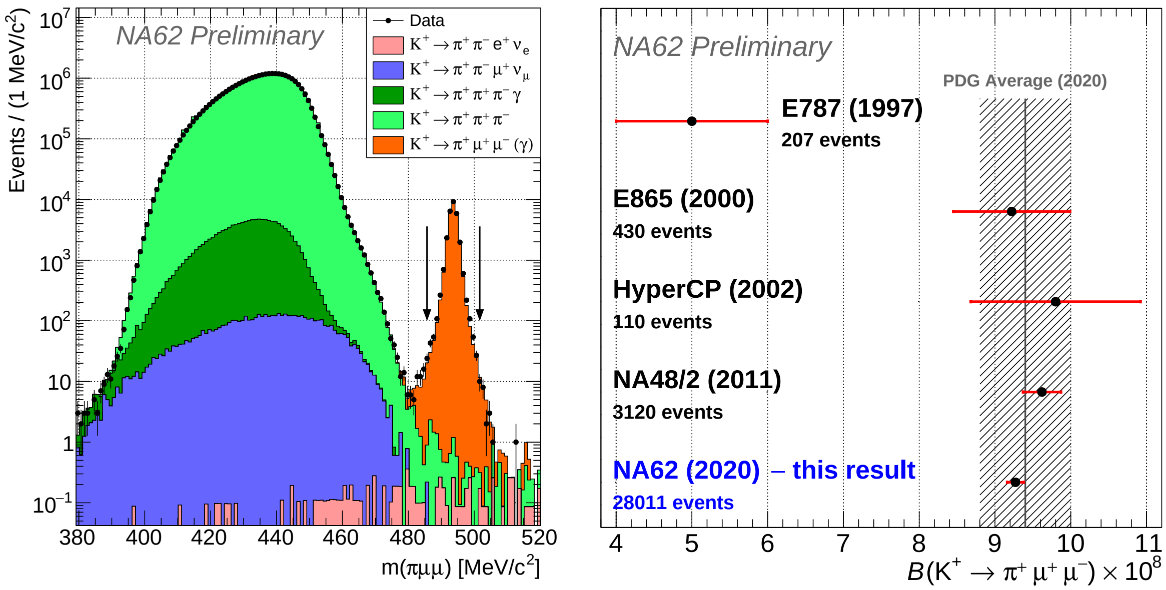

Figure 6: Left: reconstructed mass $m(\pi^+\mu^+\mu^-)$. Right: comparison of the NA62 measurement of $\mathcal{B}(K^+ \to \pi^+\mu^+\mu^-)$ with the earlier results.

which are in most cases based on the world's largest samples of these decays. Significant efforts go into the validation and improvement of the simulation of the detector response, aiming to understand and reduce the systematic uncertainties on these measurements.

The collaboration presented preliminary results from the study of the flavour-changing neutral current decay $K^+ \to \pi^+\mu^+\mu^-$ at the ICHEP 2020 conference [27]. The analysis is based on a sample of 2.8×10^4 decay candidates selected from the complete 2016–18 dataset collected with the di-muon trigger. The obtained values of form factor parameters and the branching fraction are

$$a_+ = -0.592 \pm 0.015, \quad b_+ = -0.669 \pm 0.058, \quad \mathcal{B}(K^+ \to \pi^+\mu^+\mu^-) = (9.27 \pm 0.11) \times 10^{-8}.$$

The results improve the precision of the previous leading measurement [28] by more than a factor 2 (Fig. 6), and are consistent with lepton flavour universality [29] when compared to the results of the $K^+ \to \pi^+e^+e^-$ measurements [30, 31]. A paper is in preparation.

A new measurement of the helicity-suppressed ratio $\Gamma(K^+ \to e^+\nu)/\Gamma(K^+ \to \mu^+\nu)$ [32] aims to improve on the sub-percent precision of the current best measurement [33] which would provide an important test of lepton flavour universality. The main trigger stream is used in the analysis, and the collected sample of $K^+ \to e^+\nu$ decays is several times larger than in the best measurement. Several measurements of radiative K^+ decays are in progress, providing precision tests of the predictions of Chiral Perturbation Theory describing low energy weak processes. These include the rare $K^+ \to \pi^+\gamma\gamma$ decay [34] and the radiative decays $K^+ \to e^+\nu\gamma$ and $K^+ \to \pi^0 e^+\nu\gamma$ [35, 36] recorded by the pre-scaled control and non-muon triggers, as well as the $K^+ \to \pi^+\pi^+\pi^-\gamma$ [37], $K^+ \to \pi^+\gamma e^+e^-$ [38] and $K^+ \to \ell_1^+\nu\ell_2^+\ell_2^-$ (with $\ell_{1,2} = e, \mu$) [35] decays recorded with the multi-track trigger and lepton pair triggers. NA62 has collected world's largest samples of all these decays.

Studies of neutral pion decays $\pi^0 \to e^+e^-$ and $\pi^0 \to e^+e^-\gamma$ are also in progress. Both decays proceed via the $\pi^0 \to \gamma^*\gamma^*$ vertex, described by the transition form factor which enters the computations of the hadronic light-by-light scattering contributing to the muon anomalous magnetic moment [39]. The measurement of $\mathcal{B}(\pi^0 \to e^+e^-)$ also aims to resolve the existing 2σ tension between the SM theoretical prediction [40] and the latest experimental result [41].

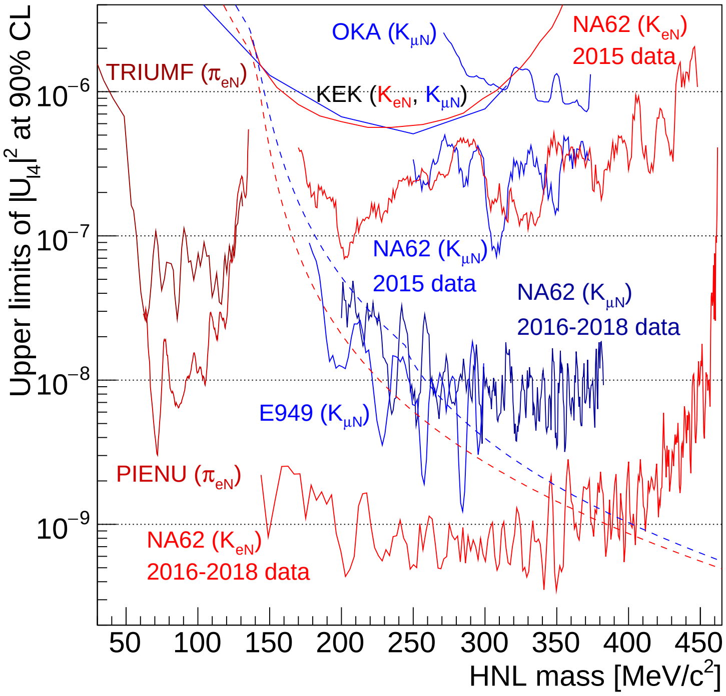

Figure 7: Summary of upper limits at 90% CL of $|U_{e4}|^2$ (red solid lines) and $|U_{\mu4}|^2$ (blue solid lined) obtained from HNL production searches in K^+ decays with the full NA62 2016–18 dataset [45, 46] and earlier production searches in $K^+ \to \ell^+ N$ and $\pi^+ \to e^+ N$ decays. The lower boundaries of $|U_{e4}|^2$ and $|U_{\mu4}|^2$ imposed by the BBN constraint [48] are shown by the lower and upper dashed lines, respectively.

The $\pi^0 \to e^+e^-\gamma$ analysis aims to improve of the measurements of the decay rate and transition form factor [42].

A comprehensive programme of searches for lepton number and lepton flavour violating K^+ decays is advancing. Following a publication of world-leading upper limits of the $K^+ \to \pi^-\ell^+\ell^+$ decay rates [43], new upper limits (at 90% CL) of the $K^+ \to \pi^\pm\mu^\mp e^+$ decay rates based on the full 2016–18 dataset have been announced at the ICHEP 2020 conference [44]:

$$\begin{aligned} \mathcal{B}(K^+ \to \pi^-\mu^+e^+) &< 4.2 \times 10^{-11}, \\ \mathcal{B}(K^+ \to \pi^+\mu^-e^+) &< 6.6 \times 10^{-11}, \end{aligned}$$

improving by an order of magnitude over the previous limits obtained by BNL experiments. A paper in preparation will also report a search for the lepton flavour violating $\pi^0 \to \mu^-e^+$ decay.

The programme of searches for heavy neutral lepton (N) production in $K^+ \to e^+N$ and $K^+ \to \mu^+N$ decays with the full 2016–18 dataset has been completed. The final results have been published [45, 46], along with the new $\mathcal{O}(10^{-6})$ upper limits of the branching ratios of the $K^+ \to \mu^+\nu\nu\bar{\nu}$ and $K^+ \to \mu^+\nu X$ decays, where X is an invisible scalar or vector hidden-sector mediator. The model-independent upper limits obtained on the lepton mixing parameters $|U_{e4}|^2$ and $|U_{\mu4}|^2$, shown in Fig. 7, improve on the previous limits from both production decay searches [47], and partially saturate the range allowed by the Big Bang Nucleosynthesis (BBN) constraint [48].

A detailed evaluation of rare decay trigger purity and efficiency has been carried out with the 2016–18 data and a full trigger simulation. This has led to the optimisation of the rare decay trigger chains for post-LS2 data collection, including reduction of the number of trigger chains and adjustment of L0 multiplicity requirements. Further improvements to the trigger purity are expected due to the inclusion of the Anti0 detector, installed during LS2, into the L0 trigger system. We expect that these refinements will allow the continuation of rare decay data collection at the increased luminosity with lower downscaling factors than in 2018.

7 Exotic processes

Thanks to its high intensity beam and detector performance (redundant particle-identification capability, extremely efficient veto system and high resolution measurements of momentum, time, and energy), NA62 can achieve sensitivities to long-lived light mediators in a variety of new-physics scenarios.

In 2020, the analysis of data taken with parasitic triggers and in the so-called beam-dump (BD) configuration progressed. In this document, as an example we will discuss specifically the progress in the background modelling for the search for ALP to di-photon decays.

A statistics equivalent to a few 10^{16} protons on target (POT) has been collected in BD mode, to allow a first, comprehensive search for exotic particle decays. The search for ALP decays to two photons is particularly advanced and should allow the exploration of a new region of the parameter space [49]. Two main sources of background have been identified:

- Muon-halo-initiated showers producing photons in the beam elements just upstream of the NA62 decay volume; these can pollute the sample for total LKr energies below 20 GeV;
- Tertiary production of K_S or Λ decaying to neutral final states, which can mimic the ALP signal for LKr energies above 20 GeV.

The challenging task of achieving an *a priori* background estimate has been tackled using biased simulation techniques, also exploiting studies ongoing within the recently restarted Physics Beyond Colliders effort. For the first source, the background estimate is being evaluated using control samples with in-time activity detected by the upstream LAV stations. For the second source, secondary K^+ mesons produced in the TAX and surviving up to the last elements of the beam line upstream of the decay volume are simulated. These K^+ can produce K_S and Λ tertiaries in the so-called final collimator. Preliminary results show agreement between the distribution shapes for data and expected background within the statistical uncertainties, when the decays $K_S \to \pi^+\pi^-$ and $\Lambda \to \pi^- p$ are reconstructed. The distributions of the K_S momentum and vertex Z-coordinate are shown in Fig. 8 for data and simulation.

A statistics equivalent to a few 10^{17} protons on target (POT) has been collected in parasitic mode to allow searches for exotic particle decays to di-muon pairs. The analysis of these data have shown that both the background from accidental activity and that from in-time track pairs is well under control. The sensitivity achievable with a future data set corresponding to a few 10^{18} POT would considerably improve on that of the present data set. The improvement in halo background rejection obtained thanks to the new Anti0 hodoscope is under evaluation.

The possibility of collecting around 10^{18} POT during the data taking in 2021 with a BD configuration has triggered a number of readiness studies. On one side, simple and easily reversible optimizations of the beam line have been defined, guaranteeing a reduction of the muon-halo background by a factor of 4 at the trigger level, see [50] for details. On the other side, an improved trigger setup has been defined, guaranteeing acceptance to visible exotic-particle decays both to charged and neutral final states, in a wider exotic mass range than before. The charged modes will be triggered requiring two or more in-time CHOD tiles, thus allowing sensitivity from the start of the kinematic threshold. The neutral modes will be triggered requiring one or more LKr energy deposits, with a threshold low enough to allow collection of a muon control sample to be exploited for quick monitoring of the efficiency of the charged trigger. The data set collected should allow sensitivities well beyond the past experiments for several model-dependent [51] and model-independent [52] physics cases.

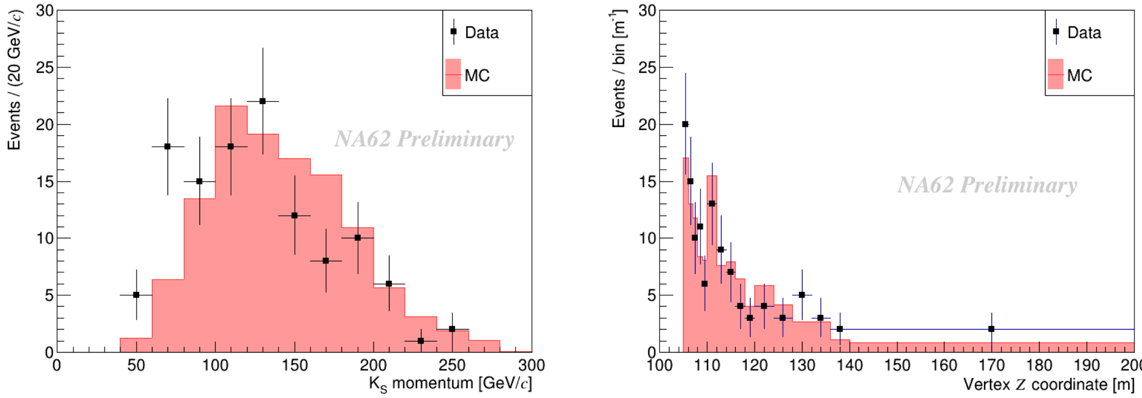

Figure 8: Distributions from reconstructed $K_S \to \pi^+\pi^-$ decays: momentum (left) and Z-coordinate of the decay vertex (right). Data corresponding to 1.6×10^{16} POT (117 events, black dots, error bars statistical only) are compared to simulation data obtained from a combination of the G4BeamLine and NA62MC Monte Carlo software (red, normalized to the data integral).

8 Publication of NA62 data

Since the last NA62 SPSC review in April 2020, the collaboration has completed the following publications:

- E. Cortina Gil et al. (NA62 collab.), An investigation of the very rare $K^+ \to \pi^+\nu\nu$ decay, JHEP 11 (2020) 42.
- E. Cortina Gil et al. (NA62 collab.), Search for heavy neutral lepton production in the K^+ decays to positrons, Phys. Lett. B807 (2020) 135599.
- E. Cortina Gil et al. (NA62 collab.), Search for π^0 decays to invisible particles, JHEP 02 (2021) 201.
- E. Cortina Gil et al. (NA62 collab.), Search for a feebly interacting particle X in the decay $K^+ \to \pi^+ X$, JHEP 03 (2021) 058.
- E. Cortina Gil et al. (NA62 collab.), Search for K^+ decays to a muon and invisible particles, CERN-EP-2021-018, arXiv:2101.12304, accepted by PLB.
- E. Cortina Gil et al. (NA62 collab.), Measurement of the very rare $K^+ \to \pi^+\nu\overline{\nu}$ decay, CERN-EP-2021-050 and arXiv:2103.15389, submitted to JHEP.

The collaboration is actively contributing to major International Conferences and topical Workshops with recently published or preliminary physics results from NA62 and NA48/2 data analyses. In the past year (May 2020 to April 2021), the collaboration speakers presented 20 plenary talks and 12 parallel talks. Although reduced with respect to the previous report, the number of contributions is still considerable given the pandemic situation and its impact on physics conferences. In particular, NA62 contributed with several results and presentations to the ICHEP2020 Conference. More contributions are already foreseen in future 2021 Conferences.

References

[1] E. Cortina Gil *et al.* (NA62 collab.), CERN-EP-2021-050, arXiv:2103.15389, submitted to JHEP

[2] Addendum I to P326, SPSC-2019-039.

[3] E. Cortina Gil *et al.* (NA62 collab.), JINST 12 P05025 (2017).

[4] BDSIM: https://doi.org/10.1016/j.cpc.2020.107200

[5] A.J. Buras, D. Buttazzo, J. Girrbach–Noe and R. Knegjens, JHEP 11, 33 (2015).

[6] G. Buchalla and A.J. Buras, Nucl. Phys. B 548, 309 (1999).

[7] A.J. Buras, M. Gorbahn, U. Haisch and U. Nierste, Phys. Rev. Lett. 95, 261805 (2005).

[8] J. Brod, M. Gorbahn and E. Stamou, Phys. Rev. D 83, 034030 (2011).

[9] G. Isidori, F. Mescia and C. Smith, Nucl. Phys. B 718, 319 (2005).

[10] F. Mescia and C. Smith, Phys. Rev. D 76, 034017 (2007).

[11] M. Blanke, A.J. Buras and S. Recksiegel, Eur. Phys. J. C 76, 182 (2016).

[12] M. Blanke, A.J. Buras, B. Duling, K. Gemmler and S. Gori, JHEP 03, 108 (2009).

[13] A.J. Buras, D. Buttazzo and R. Knegjens, JHEP 11, 166 (2015).

[14] J. Aebischer, A.J. Buras and J. Kumar, JHEP 12, 097 (2020).

[15] G. Isidori, F. Mescia, P. Paradisi, C. Smith and S. Trine, JHEP 08, 064 (2006).

[16] M. Tanimoto and K. Yamamoto, Prog. Theor. Exp. Phys. 2016, 123B02 (2016).

[17] T. Blazek and P. Matak, Int. J. Mod. Phys. A 29, 1450162 (2014).

[18] M. Bordone, D. Buttazzo, G. Isidori and J. Monnard, Eur. Phys. J. C 77, 618 (2017).

[19] C. Bobeth and A.J. Buras, JHEP 02, 101 (2018).

[20] S. Fajfer, N. Kosnik and L. Vale Silva, Eur. Phys. J. C 78, 275 (2018).

[21] R. Marchevski et al. (NA62 Collab.), PoS (ICHEP2020) 398.

[22] E. Cortina Gil et al., JHEP 03 (2021) 058.

[23] 2020 NA62 Status Report to the CERN, SPSC-SR-266.

[24] K. He, X. Zhang and J. Sun, arXiv:1512.03285v1 (2015).

[25] A.Howard et al., arXiv:1704.04861v1 (2017).

[26] W.Liu et al, arXiv:1512.02325 (2015).

[27] L. Bician *et al.* (NA62 collab.), PoS (ICHEP2020) 364.

[28] J. R. Batley *et al.* (NA48/2 collab.), Phys. Lett., **B697** (2011) 107.

[29] A. Crivellin *et al.*, Phys. Rev. **D93** (2016) 074038.

[30] R. Appel *et al.*, Phys. Rev. Lett. **83** (1999) 4482.

[31] J. R. Batley *et al.* (NA48/2 collab.), Phys. Lett., **B677** (2009) 246.

[32] V. Cirigliano and I. Rosell, Phys. Rev. Lett. **99** (2007) 231801.

[33] C. Lazzeroni *et al.* (NA62 collab.), Phys. Lett. **B719** (2013) 326.

[34] G. Ecker, A. Pich and E. de Rafael, Nucl. Phys. **B303** (1988) 665.

[35] J. Bijnens, G. Ecker, and J. Gasser, Nucl. Phys. **B396** (1993) 81.

[36] V. Cirigliano *et al.*, Rev. Mod. Phys. **84** (2012) 399.

[37] G. D'Ambrosio *et al.*, Z. Phys. **C76** (1997) 301.

[38] F. Gabbiani, Phys. Rev. **D59** (1999) 094022.

[39] M.Hoferichter *et al.*, JHEP 10 (2018) 141.

[40] T. Husek, K. Kampf and J. Novotný, Eur. Phys. J. **C74** (2014) 3010.

[41] E. Abouzaid *et al.*, Phys. Rev. **D75** (2007) 012004.

[42] C. Lazzeroni *et al.* (NA62 collab.), Phys. Lett. **B768** (2017), 38.

[43] E. Cortina Gil *et al.* (NA62 collab.), Phys. Lett. **B797** (2019) 134794.

[44] J. Swallow *et al.* (NA62 collab.), PoS (ICHEP2020) 430.

[45] E. Cortina Gil *et al.* (NA62 collab.), Phys. Lett. **B807** (2020) 135599.

[46] E. Cortina Gil *et al.* (NA62 collab.), arXiv:2101.12304, accepted for publication in Phys.Lett.B.

[47] J. Beacham *et al.*, J. Phys. **G47** (2020) 010501.

[48] A. D. Dolgov *et al.*, Nucl. Phys. **B590** (2000) 562.

[49] B. Döbrich, J. Jaeckel and T. Spadaro, JHEP **05** (2019), 213 [erratum: JHEP **10** (2020), 046]

[50] M. Rosenthal, *et al.* Int. J. Mod. Phys. A **34** (2019) no.36, 1942026

[51] J. Beacham, *et al.* J. Phys. G **47** (2020) no.1, 010501

[52] B. Döbrich, F. Ertas, F. Kahlhoefer and T. Spadaro, Phys. Lett. B **790** (2019), 537-544.